Hierarchical Self-Assembly of Di-, Tri- and Tetraphenylalanine Peptides Capped with Two Fluorenyl Functionalities: From Polymorphs to Dendrites

Enric Mayans,[1,2] Gema Ballano,[3] Jordi Casanovas,[4] Luis J. del Valle,[1,2] Maria M. Pérez-Madrigal,[1,2] Francesc Estrany,[2,5] Ana I. Jiménez,[3] Jordi Puiggalí,[1,2,*] Carlos Cativiela,[3,*] and Carlos Alemán[1,2,*]

[1] *Departament d'Enginyeria Química, ETSEIB, Universitat Politècnica de Catalunya, Diagonal 647, Barcelona E-08028, Spain*

[2] *Centre for Research in Nano-Engineering, Universitat Politècnica de Catalunya, Campus Sud, Edifici C', C/Pasqual i Vila s/n, Barcelona E-08028, Spain*

[3] *Department of Organic Chemistry and Instituto de Síntesis Quimica y Catalisis Homogenea (ISQCH), University of Zaragoza–CSIC, 50009 Zaragoza, Spain*

[4] *Departament de Química, Escola Politècnica Superior, Universitat de Lleida, c/ Jaume II nº 69, Lleida E-25001, Spain*

[5] *Departament d'Enginyeria Química, EUETIB, Universitat Politècnica de Catalunya, Comte d'Urgell 187, 08036 Barcelona, Spain*

[*] jordi.puiggali@upc.edu, cativiela@unizar.es and carlos.aleman@upc.edu

ABSTRACT

Homopeptides with 2, 3 and 4 phenylalanine (Phe) residues and capped with fluorenylmethoxycarbonyl and fluorenylmethyl ester at the N- and C-terminus, respectively, have been synthesized to examine their self-assembly capabilities. Depending on the conditions, the di- and triphenylalanine derivatives self-organize into a wide variety of stable polymorphic structures, which have been characterized: stacked braids, doughnuts-like, bundled arrays of nanotubes, corkscrew-like and spherulitic microstructures. These highly aromatic Phe-based peptides also form incipient branched dendritic microstructures, even though they are highly unstable, making their manipulation very difficult. In opposition, the tetraphenylalanine derivative spontaneously self-assemble into stable dendritic microarchitectures made of branches growing from nucleated primary frameworks. The fractal dimension of these microstructures is ~1.70, which evidences self-similarity and two-dimensional diffusion controlled growth. DFT calculations at the M06L/6-31G(d) level have been carried out on model β-sheets since it is the most elementary building block of Phe-based peptide polymorphs. Results indicate that the antiparallel β-sheet is more stable than the parallel one, the difference between them growing with the number of Phe residues. Thus, the cooperative effects associated with the antiparallel disposition become more favorable when the number of Phe residues increases from 2 to 4, while those of the parallel disposition remained practically constant.

INTRODUCTION

Fluorenylmethoxycarbonyl (Fmoc)-based short peptides are widely studied because of their particular supramolecular assembly capabilities. Thus, the Fmoc moiety provides strong aromatic interactions that drive the peptide self-assembly into nanofibers or nanotubes.[1-11] In peptide sequences containing aromatic residues, which intrinsically form π-stacking interactions, the role of such type of interactions become predominant. A very illustrative example corresponds to the self-assembly of diphenylalanine (FF), as a minimal sequence to form peptide nanostructures, which organizes forming peptide nanotubes stabilized by a combination of hydrogen bonding and repeated phenyl stacking interactions.[12-14] In contrast, Fmoc-FF forms peptide fibrils[15] and very stable hydrogels[9,16,17] that were thought to arise from the stacking between Fmoc groups and between phenyl groups. The remarkable importance of stacking interactions induced by the Fmoc group at the N-terminus was also illustrated using a series of dipeptides and amino acids,[18] such aromatic moiety acting as a consistent facilitator of gelation in comparison to other simple hydrophobic groups, such as *tert*-butoxycarbonyl.

More recently, research on the self-assembly of triphenylalanine (FFF) and Fmoc-FFF also evidenced some important differences.[19,20] More specifically, FFF and Fmoc-FFF were found to self-assemble into solid fibrillary plate-like nanostructures[19] (also named "nanoplates") and hydrogels,[20] respectively. In all cases, π-π stacking interactions between aromatic rings were found to play a decisive role in the formation of such supramolecular aggregates. In a very recent study we examined the self-assembly of tetraphenylalanine (FFFF) and Fmoc-FFFF, which had never been reported before.[21] FFFF molecules were found to assemble into tubes, exhibiting structural imperfections in comparison to FF. Theoretical calculations suggested that these

structural defects in FFFF tubes are due to the fact that the increment in the conformational flexibility is accompanied by a reduction in the number of restrictions associated with hydrogen bonds. In opposition, Fmoc-FFFF organizes into a variety of polymorphs depending on the experimental conditions, which included ultra-thin nanoplates, fibrils and star-like submicrometric aggregates.[21]

The applications of self-assembled peptides in the biomedical (*e.g.* as cargo to target delivery of drugs and genes, scaffolds in tissue engineering and regenerative biomedicine, and biosensors) and nanotechnological (*e.g.* fabrication of composite materials by controlled nucleation, electronic and magnetic nanonowires) fields have been extensively reviewed in the last years.[22-25] However, many of these applications are focused on a well-defined morphology. The control exerted by the environmental conditions in the morphology of a given system, regulating the apparition of different polymorphs, can enhance such applications, even leading to multifunctional systems. In this work we synthesize and study the self-assembly of phenylalanine-based peptides capped with Fmoc and 9-fluorenylmethyl ester (OFm) as N- and C-terminal aromatic components, respectively. More specifically, the results for a peptide series formed by FF, FFF and FFFF have been systematically compared. Furthermore, intermolecular interactions formed by these peptides, named Fmoc-FF-OFm, Fmoc-FFF-OFm and Fmoc-FFFF-OFm (Scheme 1), have been also investigated using theoretical calculations. It should be remarked that the interest of these systems lies not only in the high concentration of aromatic groups but also in the complete elimination of the normally free basic (N-terminus) and acidic (C-terminus) ends that are often important for gelation.[2,26] Accordingly, no hydrogel is *a priori* expected for these systems while the formation of multiple supramolecular self-assembled organizations may be reached through stacking interactions. It is worth noting that in a very recent study it was

reported a double Fmoc-functionalized low molecular weight peptide, which behaved very differently from the corresponding single Fmoc-functionalized analogue.[27] More specifically, Fmoc-Lys-Fmoc was found to form pH-controlled gels whereas single Fmoc-Lys failed under similar experimental conditions.

METHODS

Materials. Boc and Fmoc-aminoacids were supplied by PolyPeptide group, *N*-[3-(dimethylamino)-propyl]-*N*'-ethylcarbodiimide hydrochloride was a product from Bachem and all other reagents for peptide synthesis were purchased from Sigma-Aldrich.

Peptide synthesis and characterization.

The preparation of Fmoc-FF-OFm, Fmoc-FFF-OFm and Fmoc-FFFF-OFm peptides was carried out following standard procedures of peptide synthesis in solution starting from the corresponding F-derivative and using the Boc or Fmoc group as protection for the amino moieties. A general procedure for the coupling reactions is given in Figure 1.

Melting points were determined on a Gallenkamp apparatus and are uncorrected. IR spectra were registered on a Thermo Nicolet Avatar 360 FTIR spectrophotometer; ν_{max} is given for the main absorption bands. ^{1}H and ^{13}C NMR spectra were recorded on a Bruker AV-400 or ARX-300 instrument at room temperature unless otherwise indicated and using the residual solvent signal as the internal standard; chemical shifts (δ) are expressed in ppm and coupling constants (*J*) in Hertz. Optical rotations were measured on a JASCO P-1020 polarimeter. High-resolution mass spectra were obtained on a Bruker Microtof-Q spectrometer.

Preparation of initial solutions of peptides. Organic solvents were purchased from Sigma-Aldrich, Fisher Scientific and Scharlab. The peptide concentration in the

prepared solutions ranged from 0.05 to 5 mg/mL. Solutions or dispersions (25 or 100 μL) of the peptides were prepared from 4-5 mg/mL stocks. The solvents used to dissolve the synthesized peptides were hexafluoroisopropanol (HFIP) and dimethylformamide (DMF). Milli-Q water, methanol (MeOH), ethanol (EtOH), isopropanol (^{i}PrOH) or acetone was added as co-solvents to reduce the peptide concentration and alters the polarity of the environment. More specifically, as usual for Phe-based aromatic peptides, the three investigates compounds were soluble in HFIP and DMF, while they were only partially soluble or insoluble in alcohols, water and acetone. Accordingly, self-assembly studies were conducted using as solvents pure HFIP and mixtures HFIP:alcohol (alcohol= MeOH, EtOH and ^{i}PrOH), H_2O being added to complete the series of mixtures. As the main objective of these co-solvents was to increase the hydrophilicity of the environment and, for this purpose, the ratio solvent:co-solvent was systematically varied from 4:1 to 1:99 (*i.e.* 4:1, 2:3, 1:4, 1:9, 1:19; 1:24, 1:49 and 1:99). In addition, as peptides were also soluble in DMF and partially soluble in acetone, some trials were performed using pure DMF, DMF:acetone and HFIP:acetone mixtures, even though in this case the number of explored ratios was lower because the amount of observed microstructures was relatively infrequent with respect to HFIP and HFIP:alcohol. Finally, 10 or 20 μL aliquots were placed on microscope coverslips or glass slides (glass sample holders) and kept at room temperature (25 ºC) or inside a cold chamber (4 ºC) until dryness. The humidity was kept constant in both laboratories at 50%.

Optical microscopy. Morphological observations were performed using a Zeiss Axioskop 40 microscope. Micrographs were taken with a Zeiss AxiosCam MRC5 digital camera.

Scanning electron microscopy (SEM). SEM studies were performed in a Focussed Ion Beam Zeiss Neon 40 scanning electron microscope operating at 5 kV and equipped with an EDX spectroscopy system. Samples were mounted on a double-side adhesive carbon disc and sputter-coated with a thin layer of carbon to prevent sample charging problems.

Atomic Force Microscopy (AFM). Topographic AFM images were obtained using either a Dimension 3100 Nanoman AFM or a Multimode, both from Veeco (NanoScope IV controller) under ambient conditions in tapping mode. AFM measurements were performed on various parts of the morphologies, which produced reproducible images similar to those displayed in this work. Scan window sizes ranged from 5×5 μm^2 to 80×80 μm^2.

Fractal characterization of dendritic microstructures. The dendritic assembly behavior of Fmoc-FFFF-OFm was observed by optical microscopy and AFM. The fractal dimension of the dendritic morphology was determined by the fractal box-counting method[28] using ImageJ software version 1.50e. (version: 2.0.0-rc-43/1.50e, Fiji package).[29] For this analysis, AFM images of dendritic microstructures were converted into 8-bit binary format images, which were covered by square box arrays. The number of boxes occupied by the underlying dendritic morphology (N) and the side length of boxes (L) were plotted in logarithmic scale to determine the fractal dimension (FD) of the dendrites.

Theoretical calculations. Density Functional Theory (DFT) calculations were performed using the Gaussian 09 computer package.[30] The geometries of the different investigated systems were fully optimized using the M06L[31,32] functional, which was developed by Zhao and Truhlar to account for dispersion, combined with the 6-31G(d) basis set. No symmetry constraints were used in the geometry optimizations.

The interaction energy, ΔE_{int}, for each complex formed by three peptide molecules was computed as the difference between the energy of the complex and the sum of the energies calculated for each of the three peptide molecule:

$$\Delta E_{int} = E(complex) - E(peptide\ 1) - E\ (peptide\ 2) - E(peptide\ 3) \quad (1)$$

The cooperative energy, ΔE_{coop}, for the β-sheets formed by three strands was estimated as the difference between ΔE_{int} and the expected interaction energies (Eq. 2). The expected interaction energy, $\Delta E_{int}(E)$, was supplied as the sum of the DFT interaction energies of all dimers contained in the complex (Eqs. 3-6). Accordingly, ΔE_{coop} provides an evaluation of the many-body (non-additive) effects.

$$\Delta E_{coop} = \Delta E_{int} - \Delta E_{int}(E) \quad (2)$$

$$\Delta E_{int}(E) = \Delta E_{int}\ (1\text{-}2) - \Delta E_{int}\ (2\text{-}3) - \Delta E_{int}\ (1\text{-}3) \quad (3)$$

$$\Delta E_{int}\ (1\text{-}2) = E(dimer\ 1\text{-}2) - E(peptide\ 1) - E(peptide\ 2) \quad (4)$$

$$\Delta E_{int}\ (2\text{-}3) = E(dimer\ 2\text{-}3) - E(peptide\ 2) - E(peptide\ 3) \quad (5)$$

$$\Delta E_{int}\ (1\text{-}3) = E(dimer\ 1\text{-}3) - E(peptide\ 1) - E(peptide\ 3) \quad (6)$$

Interaction and cooperative energies were corrected with the basis set superposition error (BSSE) by mean of the standard counterpoise method.

FTIR spectroscopy. Infrared transmittance spectra were recorded with a Jasco FTIR 4100 Fourier Transform spectrometer in a 4000-650 cm^{-1} interval. An MKII Golden Gate attenuated total reflection (ATR) accesory from Specac was used. The measurements were taken using 4 cm-1 resolution and 1000 scans averaging.

RESULTS AND DISCUSSION

Results presented in this work only correspond to the conditions in which stable microstructures (*i.e.* microstructures that remained formed upon manipulation for optical microscopy, SEM and AFM observations) were formed. As the hydrophobicity and degree of solubility of the peptides change with the number of Phe residues, in many cases different peptides require different solvent:co-solvent ratios to self-assemble into the microstructures with similar morphologies. This feature is reflected in Table 1, which summarizes and compares the conditions required by Fmoc-FF-OFm, Fmoc-FFF-OFm and Fmoc-FFFF-OFm for the formation of stable assemblies. It is worth noting that for the three peptides under study the number of observed structures at 4 ºC is significantly higher than that at 25 ºC (*i.e.* only one stable assembly was identified for each peptide at 25 ºC). This result clearly indicates that the self-assembly of highly hydrophobic peptide molecules to form microstructures is a thermodynamically controlled process.

Peptide synthesis

To a solution of the appropriately N^{α}-protected α-amino acid (4.00 mmol) in CH_2Cl_2, 1-hydroxybenzotriazole (HOBt) (4.40 mmol) was added, and the solution was cooled to 0 ºC in an ice bath. *N*-[3-(dimethylamino)-propyl]-*N*'-ethylcarbodiimide hydrochloride (4.40 mmol) was added, followed by the solution of the amino component (4.40 mmol) in CH_2Cl_2, obtained after acidolytic removal of the protecting group and *N*-methylmorpholine (NMM) (4.40 mmol) or *N*-ethyldiisopropylamine (DIPEA) (4.40 mmol). The reaction mixture was stirred for 1 h at 0 ºC, then at room temperature for 24 h, by keeping the pH (moistened pH paper) at 8. The reaction mixture was repeatedly washed with 5% $KHSO_4$, 5% $NaHCO_3$ and water. The organic phase was dried over

$MgSO_4$ and evaporated to dryness. The peptide product was purified by flash chromatography. Boc-F-OFm was purified using a 8:2 mixture of hexane/ethyl acetate. Boc-FF-OFm and Boc-FFF-OFm were purified using a 98:2 mixture of dichloromethane:methanol while a 98:3 mixture was used for Boc-FFFF-OFm. Fmoc-containing peptides were very insoluble, precipitating upon solvent concentration. All Fmoc-containing peptides were washed with ethyl acetate. For chemical characterization, a small amount was purified using a 98:2 or 97:3 mixture of dichloromethane:methanol.

Description of all intermediates is provided in the Electronic Supporting Information (ESI).

Self-assembly of Fmoc-FF-OFm

Table 1 summarizes the different conditions required for the formation of the morphologies identified in this work. Accordingly, assemblies with different morphologies were obtained from solutions of Fmoc-FF-OFm in HFIP alone or mixed with a co-solvent. Morphology drastically depends not only on the co-solvent but also on the peptide concentration and temperature. This is evidenced in Figure S1, which displays optical micrographs of the most representative morphologies. This enormous morphological variability is in contrast with observations on Fmoc-FF, which tends to self-assemble into a hydrogel based on π-π interlocked β-sheets.[6]

Fmoc-FF-OFm assembles into stacked braid-like microstructures in 2:3 and 1:9 HFIP:water at 4 ºC and peptide concentrations ranging from 0.5 to 2 mg/mL (Figures 2a and 2b). The length and width of the braids clearly decrease with the peptide concentration in the solution, inducing a higher degree of compactness in the whole aggregate. The very compact nature of the stacked aggregate obtained for a

concentration of 0.5 mg/mL is reflected in the AFM topographic images (Figure 2b). Sonication of the solutions with a peptide concentration of 2 mg/mL reduced the lateral staking among the braids increasing the separation between them (Figure 2a), whereas the system with 0.5 mg/mL remained practically unaltered. This observation is fully consistent with the fact that the compactness of the supramolecular assemblies increases with decreasing peptide concentration. Very similar assemblies were obtained in mixtures with a high content of MeOH, *e.g.* 1:49 and 1:99 HFIP:MeOH, at 4 ºC and concentrations ranging from 0.04 to 0.1 mg/mL as is evidenced by representative optical (Figure S1c) and SEM (Figure S2a) micrographs.

Reduction of the proportion of water co-solvent in the mixtures with HFIP led to the formation of doughnut-like microstructures (Figure S1d) of different diameters (*i.e.* from ~4 to ~10 μm). The most remarkable characteristic of this morphology is the extremely high surface area, which is expected to facilitate its interaction with other molecules or even with living organisms present in the environment. Detailed inspection of these hollow microstructures (Figure 2c) reveals features very similar to those previously described for polymeric systems prepared using a micelle formation mechanism with gas bubbles templates.[33] Also, macroporous honeycomb scaffolds were successfully fabricated through the self-assembly of FF using the breath figure method, in which moist air/water droplets were responsible for the pore formation.[34] Although in this work the central hole of doughnuts-like microstructures formed from Fmoc-FF-OFm may be also due to nucleation of the assemblies around an air bubble, detailed observation of the micrographs suggests an alternative mechanism: the coexistence of small gelatinous rounded aggregates with irregular micrometric assemblies in the same samples (Figures S1d-right and S2b) indicates that their collapse gives place to the nucleation center and the subsequent growing of the doughnuts-like microstructures.

Thus, the formation of external filled region seems to precede the appearance of the hole (Figure S2c). It should be noted that the presence of gelatinous rounded aggregates is supported by the role played by aromatic end groups as facilitators of gelation.[9,16-18] Accordingly, the majority of the peptide molecules located at the central region of such gelatinous structures could migrate through diffusion towards the external region, allowing the development of the hollow microstructure after solubilization or precipitation of the remaining peptide molecules.

This proposed mechanism agrees with the recent observations of Ulijn and co-workers[35] for Fmoc-Ser-Phe-OMe (Fmoc-SF-OMe), which combines hydrophilic and hydrophobic amino acids. Fmoc-SF-OMe gave rise to spherulitic structures of several hundred microns in diameter surrounded by non-spherulitic areas of material, which was constructed of layered lamellar structures. Interestingly, nucleation points were not detected in such spherulitic structures, which is consistent with our observations for Fmoc-FF-OFm. The main difference between the microspherulites reported for Fmoc-SF-OMe[35] and the doughnuts-like assemblies obtained in this work for Fmoc-FF-OFm refers to the migration of the peptide molecules located at the center of the latter microstructures. Taking into account the large hydrophobicity of Fmoc-FF-OFm, this diffusive migration has been considered as a solvent-induced phenomenon to promote favorable peptide-solvent interactions.

Besides, birefringent microtubes are obtained in 4:1 HFIP:^{i}PrOH and 4:1 HFIP:acetone using 3-4 mg/mL peptide concentrations (Figures S1e and S1f, respectively). Although the thickness of the tubes obtained in HFIP:^{i}PrOH varies from 1 to 10 μm, all them exhibit a very smooth and regular surface. For instance, SEM micrographs and AFM images displayed in Figure 3a correspond to a tube with a thickness of 7 μm. As it can be appreciated in the high magnification SEM micrograph,

tubes present a hexagonal-like symmetry that resembles that found for well-ordered microtubes formed by self-assembled FF.[36,37] The formation of robust hexagonal microtubes was attributed to the confined organization of nanoscale tubular structures at long range during slow crystallization or aggregation (*i.e.* kinetic control of nucleation and growth).[37,38] In general, FF-based nanotubes prepared at room temperatures by rapid dispersion of molecules exhibit circular shape that is thermodynamically more stable.[12,21,39]

Hexagonal-like peptide microtubes were also obtained in 4:1 HFIP:acetone at low temperature (Figure 3b). Interestingly, high magnification SEM images recorded for the broken end of a single microtube reveal substructures (*i.e.* nanotubes) that are confined and uniaxially oriented along the longitudinal axis of the hexagonal microtube. Thus, the microtube consists of bundled arrays of nanotubes with a diameter lower than 100 nm. Therefore, these microscale hexagonal tubes result from the supramolecular organization of such nanotubular structures contained in the array. The hierarchical evolution from the molecular level to hexagonal-like microtubes through the ordered bundling of nanotubular substructures is in excellent agreement with the kinetic control of nucleation and growth discussed above.

In addition to stacked braids, microdoughnuts and microtubes, incipient branched dendritic-like microstructures were obtained from 2:3 HFIP:water and 1:4 HFIP:EtOH solutions with relatively diluted peptide concentrations after sonication (Figures S3). Nevertheless, the stability of these dendritic microstructures, which formed very rapidly only after perturbing the equilibrium conditions (i.e. removal of the upper thin glass cover of the glass slip), was very poor, thus disappearing after only ~15 min. In spite of such instability, these results suggest that Phe-based peptides could be used to tune the morphology of macromolecules and inorganic materials. In a recent study Tendler and

co-workers[40] described FF unstable dendritic structures obtained by spin-casting a HFIP peptide solution (0.5 or 1 mg/mL) onto mica. However, such morphologies, which transformed into needle-like crystals upon exposure to humid air, corresponded to star-like dendritic assemblies rather than tree-like structures like those displayed in Figure S3. Highly ordered dendritic assembly of FF was also reported by Kim and co-workers,[41] who used a buffer peptide solution with pH= 1 and a silicon wafer substrate. In this case, the morphology of the self-assembled dendrites, which resembled ice crystal structures in snowflakes,[42] was also very different from the tree-like arrangements achieved for Fmoc-FF-OFm. The instability of the dendritic structures formed by Fmoc-FF-OFm has been attributed to the effects induced by the environmental humidity and the surface charge, which experienced drastic changes when the cover glass slide was removed.

Self-assembly of Fmoc-FFF-OFm

Although previous experiments on Fmoc-FFF proved that such peptide self-assembles hydrogels,[42] a variety of morphologies have been obtained for Fmoc-FFF-OFm solutions using HFIP alone or mixed with a co-solvent (Table 1). Again, the morphology changes not only with the co-solvent but also with the peptide concentration and temperature. Optical micrographs of the most representative morphologies are provided in Figure S4. A result that deserves special attention is the apparition of dendritic-like microstructures in HFIP:EtOH mixtures (Figure S4e) that resemble those observed for Fmoc-FF-OFm (Figure S3). Unfortunately, all the dendritic-like microstructures achieved for Fmoc-FFF-OFm were very unstable, disappearing when the glass slip were manipulated for AFM and SEM characterization.

As occurred for the FF-derivative, Fmoc-FFF-OFm self-assemble into stacked braids from 1:4 HFIP:water at 4 ºC (Figures 4a and S4a), even though in this case such morphology was only detected for peptide concentrations relatively low in comparison to those found for Fmoc-FF-OFm (*i.e.* ≤ 1.0 mg/mL). Despite this difference, the degree of staking in the microstructures apparently increases with decreasing peptide concentration: Figure 4a compares SEM micrographs of stacked braids formed at 1.0 and 0.05 mg/mL. Thus, the degree of compactness is significantly higher for the aggregate formed using the lowest peptide concentration. Stacked braids with a similar morphology were also found in HFIP:EtOH (Figure S5a) at 4 ºC for low peptide concentrations. However, the most striking feature in these solvent mixtures is that stacked braids frequently form supramolecular structures at higher peptide concentrations, giving rise to three-dimensional morphologies. This is evidenced in Figures 4b and 4c, which display corkscrew-like microstructures observed for peptide concentrations of 2 and 1 mg/mL, respectively. In all the cases the evolution of the twist defined by the spirals follow a counter-clockwise sense. It is worth noting that the corkscrew-like microstructure shown in Figure 4c is attached to a hollow micro-conical structure. Moreover, inspection of the magnified SEM micrograph (inset) clearly shows that the stacked braids elements curl. Staked braids are also intuited in the 3D AFM image. For this system, stable doughnuts-like microstructures were not formed reducing the amount of co-solvent.

HFIP: ^{i}PrOH did not promote the formation of assemblies for peptide concentrations higher than 0.5 mg/mL, whereas morphologies apparently similar to those displayed in Figure 4a were obtained below this threshold (Figure S5b). However, detailed inspection reveals that such morphology does not correspond to stacked braids but to fused microfibers. In opposition, diluted solutions of Fmoc-FFF-OFm in HFIP:water at

4 ºC produced well-defined individual tubes of submicrometric diameter, as it is evidenced for a concentration of 0.05 mg/mL in Figure 4d. Moreover, as occurred for Fmoc-FF-OFm, high magnification micrographs evidence that such structures are build up through a hierarchical self-similar assembly process, according to which nanotubes with a diameter lower than 100 nm organize by growing in submicrometic-sized tubular patterns. The assembly or bundling of Fmoc-FFF-OFm nanotubes into submicroscale tubes was also observed for concentrated peptide solutions (*e.g.* 6.1 mg/mL) in 38:11 DMF:MeOH (Figure S5c).

Reduction of the amount of co-solvent in the mixtures led to drastic morphological changes, thus evidencing the strong effect of the environment on the self-assembly process, especially at the supramolecular level. For example, although stacked braids (Figure 4a) and microtubes (Figure 4d) were obtained in 1:4 and 1:99 HFIP:water at 4ºC, respectively, reduction of the water co-solvent to 4:1 HFIP:water leads to the formation of spherulitic craters (Figure S4d). Inspection of the corresponding SEM and AFM micrographs (Figure 5a) indicates that the internal and external diameters of those craters are ~3 and ~11 μm, respectively. Furthermore, the spherulitic morphology actually consists of a dense packing of short and ultra-thin nanofibers, which group around a central hole. Finally, birefringent spherulites are obtained after complete removal of the co-solvent. Interestingly, these compact disc-like assemblies, which are illustrated in Figure 5b for a 5 mg/mL peptide solution in HFIP at 4ºC, can be described as a very dense tissue of nanofibers. Birefringent spherulitic structures without nucleation points at their centers were obtained through enzymatically induced hierarchical self-assembly of Fmoc-SF-OMe.[35] Furthermore, peptide based spherulitic structures have been also prepared by solvent-induced phase transitions[43] and hierarchical assembly of aromatic peptide amphiphiles.[44]

Self-assembly of Fmoc-FFFF-OFm

Optical micrographs of the most representative assemblies identified for Fmoc-FFFF-OFm are displayed in Figure S6. Although in this case the variety of polymorphic structures decreases with respect to Fmoc-FFF-OFm and, especially, Fmoc-FF-OFm (Table 1), it should be emphasized that Fmoc-FFFF-OFm exhibits a clear tendency to form hierarchical dendritic assemblies. The stability and large surface area of the assembled morphologies make the dendritic growth of this tetrapeptide potentially useful for advanced micro- and nanofabrication.

Sonication of HFIP:water solutions at 4 ºC with low peptide concentrations (0.1-0.2 mg/mL) promoted the formation of ultra-thin dendritic-like structures, like those displayed in Figures S6a and 6a. These morphologies, which are observed through the dark-field mode in the reflected light microscopy, have been attributed to heterogeneities (*i.e.* phase-separation phenomena) involved in polycrystalline growth patterns.[45,46] More specifically, dendritic-like structures reflect an interplay between the ordering effect of crystallization and the disordering effect of interfacial instabilities. Thus, in absence of growth front nucleation processes, crystallization is known to yield highly symmetric dendrites, whereas intricately structured and locally disordered polycrystalline spherulite patterns often form.[47] Structures displayed in Figures S6a and 6a have intermediate complexity between these two extreme morphologies. The ultra-thin nature of such dendritic structures is proved by the AFM amplitude images included in Figure 6a. Moreover, inspection of the dewetting patterns in both Figures S6a and 6a suggests the presence of fractal-like holes. Dewetting at the peptide surface occurs via a nucleation and growth mechanism involved in the formation of the ultra-thin dendritic-like structures, while the formation of fractal holes has been attributed to

the anisotropy of peptide mobility induced by the solvent. Similar dewetting patterns were identified in thin films of poly(styrene)-block-poly(methyl methacrylate) diblock copolymer after annealing in block selective solvent vapor.[48]

Besides, Fmoc-FFFF-OFm molecule self-assemble forming stacked braids morphologies, similar to those reached for the smaller peptides, in 1:99 to 1:9 HFIP:EtOH at 4 ºC and peptide concentrations ranging from 0.05 to 0.5 mg/mL (Figures S6b and 6b). The length of the braids, which ranged from 9 to 16 μm, was practically independent of the peptide concentration (Figure 6b and S7). Interestingly, higher concentrations provoked the assembly of peptide molecules in soft and meta-stable dendritic-like architectures (Figure S6c). Although the formation of such assemblies was highly repetitive, they frequently disappeared in the conditions required for AFM and, especially, SEM characterization.

The most spectacular assembly was obtained for peptide 1:4 HFIP:EtOH solutions at room temperature. In this case, well-defined multidimensional dendritic microarchitectures were obtained, as it is shown in **Figure 7** for the 0.5, 1 and 2 mg/mL Fmoc-FFFF-OFm solutions. These structures appeared very fast and spontaneously by rubbing a dried mass of the material obtained from the drop-cast of the peptide in the alcohol mixture with a glass slip. Although these branched structures present some irregularities, inspection of the AFM images suggest that in the early stage of growth primary frameworks were nucleated from the center. Thus, these framework structures exhibit a 4-fold pseudo-symmetry with a typical branching angle of ~90º. As growth continued, the dendrites formed highly branched structures with a specific branching angle of ~45º. Branching angles are schematically depicted in Figure 7 for the dendritic structure derived from the 1 mg/mL peptide solution, which exhibits the highest regularity. Finally, it is worth noting that the length of branches decreases with

increasing distance from the primary framework, evidencing that the self-similarity of these hierarchical microarchitectures is not very high.

It should be mentioned that polymorphism was also reported for Fmoc-FFFF.[21] In HFIP:water this *N*-Fmoc-protected peptide was found to assemble into ultra-thin nanoplates that aggregate in microclusters. Replacement of water by EtOH as co-solvent resulted in the formation of peptide fibrils at peptide concentrations < 0.5 mg/mL, while irregular star-like structures of submicrometric dimensions appeared at higher peptide concentrations. Finally, poorly defined nanospherical aggregates were obtained at Fmoc-FFFF concentrations of 1 mg/mL in HFIP:water.

Fractal analysis of Fmoc-FFFF-OFm dendritic microarchitectures

In this section we introduce a fractal analysis of the geometrical structures of the dendritic microarchitectures obtained for Fmoc-FFFF-OFm. Fractal objects are self-similar structures for which increasing magnifications reveal similar features on different length scales.[49] The fractal dimension (*FD*), which indicates how a fractal pattern changes with the scale at which it is measured, was determined by the box-counting method[9] analyzing binary images (Figure S8) derived from the AFM images displayed in Figure 7.

Figure 8 shows logarithm plots of the number of squares boxes that occupy at least part of the dendritic microstructure (*N*) as a function of the side length of the square box (*L*). The scaling relationship $N(L) \sim L^{-FD}$ relates *FD* with slope in the logarithmic scale (*m*) through the $FD = -m$. From the slopes in Figure 8, *FD* ranges from 1.69 to 1.71 reflecting the self-similarity (*i.e.* dimensional consistency at different length scales) of the dendritic microstructures formed by Fmoc-FFFF-OFm. Furthermore, these *FD* values are very close to the ideal value of 1.67 expected for microstructures generated

by diffusion limited aggregation (DLA) onto a 2D substrate surface.[50,51] According to this, in Fmoc-FFFF-OFm 1:4 HFIP:EtOH solutions, peptide molecules or small aggregates diffuse by Brownian motion and a random walk process occurs until they contact and adhere to another one. This process, which occurs multiple times to form clusters, is dominated by steric constraints and short-range forces and, therefore, a diffusing molecule or small aggregate is more likely to adhere to the outer edges of the growing cluster than to the internal regions. The steric shielding of the internal regions of the clusters is responsible for the formation of dendritic microstructures that are fractal.

Theoretical calculations

Density Functional Theory (DFT) calculations at the M06L/6-31G(d) level have been performed on Fmoc-FF-OFm, Fmoc-FFF-OFm and Fmoc-FFFF-OFm assemblies to evaluate both the effect of the peptide length in the binding energy and the preferences of the strands within the β-sheet. It should be remarked that the M06L is a meta-hybrid generalized gradient approximation (GGA) functional with a very good response under dispersion forces, improving one of the biggest deficiencies in DFT methods.[31,32] Thus, the M06L functional is able to describe the geometry and interaction energy of complexes stabilized by non-covalent interactions, including π-staking, with accuracy close to that of couple cluster calculations with both single and double substitutions.

Starting conformations for Fmoc-FF-OFm, Fmoc-FFF-OFm and Fmoc-FFFF-OFm were taken from a previous DFT study on *n*-Phe homopeptides with *n* ranging from 1 to 4.[52] As those calculations were performed considering acetyl (Ac) and *N*-methylamide (NHMe) as N- and C-terminal groups, these have been replaced by Fmoc and OFm,

respectively, all the resulting structures being re-optimized at the M06L/6-31G(d) level. After this, the three lower energy conformations of each peptide were used to construct assemblies involving three identical molecules arranged in parallel or antiparallel orientations defined with respect to the molecule. Around 20-30 starting complexes were obtained as for each peptide, complete geometry optimizations being conducted for all them at the M06L/6-31G(d) level.

Although the three minimum energy conformations considered for Fmoc-FF-OFm, Fmoc-FFF-OFm and Fmoc-FFFF-OFm peptides in the starting complexes did not correspond to the semi-extended β-strands,[52] geometry optimizations led to the β-sheet alignment of three β-strands as the most stable complex for both parallel and antiparallel assemblies. The most important characteristics associated with such lowest energy β-sheet dispositions are summarized in Table 2 for each peptide, while Figures 9, S9 and S10 represent such structures for Fmoc-FF-OFm, Fmoc-FFF-OFm and Fmoc-FFFF-OFm, respectively. In the parallel disposition the phenyl side groups of all strands are perfectly packed forming aromatic π-ladders, while the phenyl groups of consecutive strands point in opposite directions in the antiparallel arrangement. The number of intermolecular hydrogen bonds in Fmoc-FF-OFm, Fmoc-FFF-OFm and Fmoc-FFFF-OFm is 2, 3, and 4, respectively, per pair of interacting molecules either in parallel or antiparallel. However, in all cases hydrogen bonding parameters, especially the H···O distance, are more favourable for the antiparallel than for the parallel assembly. This feature agrees with the fact that the antiparallel sheet is energetically favoured with respect to the parallel one for the three investigated peptides. Moreover, the instability of the parallel assembly increases from 1.8 to 9.8 kcal/mol when the number of Phe residues in the peptide increases from 2 to 4. This behavior is fully consistent with the interaction energies (ΔE_{int}) listed in Table 2, which only take into

account the non-covalent interactions between the three peptides of each system. Thus, the ΔE_{int} values calculated for the antiparallel / parallel assemblies decrease from -52.8 / -51.0 kcal/mol to -88.6 / -78.7 kcal/mol when the number of Phe per molecule increases from 2 to 4.

The cooperative energy (ΔE_{coop}) values for all complexes, which were calculated as it is described in the ESI, are included in Table 2. It should be noted that ΔE_{coop} provides an evaluation of the many-body non-additive effects. Amazingly, the ΔE_{coop} values obtained for the parallel assembly of the three peptides are very similar, ranging from -7.5 (Fmoc-FF-OFm and Fmoc-FFF-OFm) to -8.3 kcal/mol (Fmoc-FFFF-OFm). In contrast, for the antiparallel assembly, ΔE_{coop} gradually decreases from a repulsive value of +1.5 kcal/mol for Fmoc-FF-OFm, which is consistent with the presence of anti-cooperative effects, to -4.9 kcal/mol for Fmoc-FFFF-OFm. Accordingly, representation of both the relative energy between the parallel and antiparallel arrangements (ΔE) and the difference between their ΔE_{coop} values [$\Delta\Delta E_{coop}$= ΔE_{coop}(antiparallel) – ΔE_{coop}(parallel)] against the number of Phe residues (Figure S11) clearly indicates that the stability of the antiparallel assembly with respect to the parallel one increases with the size of the homopeptide.

The antiparallel preferences of the three peptides studied in this work have been proved by FTIR spectroscopy. More specifically, FTIR spectra were registered considering two different samples of each peptide: (i) fibrous self-assembled structures; and (ii) quenched samples coming from (i) (*i.e.* fibrous structures were melted at 210-260 ºC and immediately cooled using liquid nitrogen to avoid the crystallization and/or formation of ordered structures). Comparison of the spectra recorded for the two samples of Fmoc-FF-Fmoc (Figure S12) confirms the tendency of this peptide to self-assemble into antiparallel β-sheets. Thus, fibrous samples exhibit sharp peaks at 1617

and 1695 cm^{-1}, which have been related with the presence of β-sheet structures and with an antiparallel arrangement of the β-sheets, respectively.[53] However, although the positions of these two peaks are typical to an antiparallel arrangement of the β-sheets, their relative intensity is not. Thus, for ideally defined antiparallel β-sheet arrangements, usually find in longer peptide sequences and proteins, the band at 1695 cm^{-1} is expected to be much weaker.[54] This unusual feature was also detected for the Fmoc-FF[26] and, by analogy, has been attributed to the short peptide sequence. Thus, the antiparallel β-sheet obtained for these two amino acids peptide (Fmoc-FF-Fmoc and Fmoc-FF) is not ideal.[26] Interestingly, the spectra recorded for fibrous Fmoc-FFF-Fmoc and Fmoc-FFFF-Fmoc samples also display the peak at 1695 cm^{-1}, even though in these cases a very intense peak appears at 1640-1645 cm^{-1} (Figure S13). The latter absorption, which has been also identified in fibrous amyloids organized in antiparallel β-sheets,[55] is related with the twist angle of β-sheets formed by a large number of β-strands. These observations are fully consistent with previously discussed theoretical calculations.

Significant findings are also detected from the comparison of the antiparallel preferences found in this work for Fmoc-FF-OFm, Fmoc-FFF-OFm and Fmoc-FFFF-OFm with those of their unblocked homologues or with a single Fmoc group. Thus, X-ray crystallography proved a parallel β-sheet assembly for FF,[56] while which was confirmed by FTIR studies.[57] In contrast, intermolecular hydrogen bonds and anti-parallel sheets were found for Fmoc-FF.[6] This change was attributed to the interlocking the Fmoc groups from alternate β-sheets to create π-stacked pairs. On the other hand, Tamamis *et al.*[42,58] and Guo *et al.*[59] used atomistic and coarse-grained molecular dynamics (MD) simulations, respectively, to study the assembly mechanism and the molecular basis for the structural features of FFF-based peptides nanostructures. Authors found that FFF-based peptides spontaneously assembled into solid nanometer-

sized nanospheres and nanorods with substantial content of anti-parallel β-sheet. Furthermore, theoretical calculations on FFFF and Fmoc-FFFF using the methodology that in the present study revealed a parallel β-sheets for FFFF and Fmoc-FFFF.[21] The overall of those previous observations combined with the results presented in work indicate that the β-sheet assembly of Phe-based peptides depends on their hydrophobicity, which in turn varies with both the number of Phe residues and the presence of one or two Fmoc groups. Accordingly, it can be concluded that π-stacking interactions are the driving force for the formation of β-sheet assemblies in Fmoc-containing peptides.

Quantitative prediction of 2D and 3D assemblies combining a bottom-up approach with atomistic computer simulations is a very complex task. Thus, although the rational design of molecules for biological and pharmaceutical applications is rather well established, only few works predict the complete self-assembly of soft materials using computational tools.[30,31,60,61] Experimental observations presented in this work for small Phe-homopeptides with two fluorenyl functionalities reveal that their self-assembly is greatly influenced by both the solvent and the peptide concentration, which further complicates the prediction of their 3D structure. Because of this, no attempt has been carried out in this work to extend the antiparallel 1D model predicted for Fmoc-FF-OFm, Fmoc-FFF-OFm and Fmoc-FFFF-OFm to 2D packing of β-sheets.

CONCLUSIONS

Self-assembled structures in the nano- and microscale are central for future technological applications. Within this context peptide assemblies are of special interest for the nanoscience and biomaterials science communities. Following our previous work, which proved the importance of N- and C-termini capping groups in the ordered

assemblies of di-, tri- and tetraphenylalanine motifs, the current work has explored the self-assemblies of highly aromatic peptides by capping the N- and C-terminal ends of Phe-derivatives with fluorenylmethoxycarbonyl and fluorenylmethyl ester, respectively.

Specifically, we have reported the spontaneous formation of a large number of stable polymorphic structures for Fmoc-FF-OFm, Fmoc-FFF-OFm and Fmoc-FFFF-Fmoc. Thus, depending on the solvent:co-solvent conditions, peptide concentration and temperature, molecules can organize into stacked braids, doughnuts-like, bundled arrays of nanotubes, corkscrew-like and/or spherulitic microstructures. In addition to these well-organized structures, such three small bioinspired molecules exhibit some ability to assemble into dendritic assemblies of various sizes. Unfortunately, the dendritic structures formed by Fmoc-FF-OFm and Fmoc-FFF-OFm were unstable; they rapidly disappeared when the equilibrium conditions were slightly perturbed. On the contrary, very stable well-defined dendritic structures are derived from 0.5-2 mg/mL Fmoc-FFFF-OFm solutions in 1:4 HFIP:EtOH at room temperature. AFM images have revealed that they consisted of a central framework with 4-fold pseudo-symmetry that grows forming highly branched structures. The fractal dimension analysis used in this work reflects not only self-similarity but also that the dendritic assembly occurs through a diffusion limited aggregation mechanism onto a plane (*i.e.* the surface substrate).

Theoretical calculations considering a model β-sheet with three interacting strands indicate that the studied peptides adopt an antiparallel arrangement, which is more stable than the parallel one, with intermolecular hydrogen bonds and π-π interactions. Moreover, such stability increases with the length of the Phe-segment. Unfortunately, extension of these theoretical studies to 2D and/or 3D nano-architectures represents a very complex task that, in addition, is severely limited by the large influence of the

environmental conditions (*e.g*. solvent, peptide concentration and temperature) in the assembly.

In summary, our results suggest that Phe-homopeptides capped with two fluorenyl functionalities are a novel class of material that can be used to achieve a wide variety of desirable structures at the very small length-scale by simply controlling the assembly conditions. In particular, the well-defined and stable dendritic structures formed by Fmoc-FFFF-OFm indicate that highly aromatic Phe-homopeptides with four, or even more, residues should be considered as powerful building blocks for the fabrication of complex and relatively infrequent structures. Potential applications of peptide assemblies in nanotechnology and nanobiology should be explored along next decades.

Acknowledgements

Authors thank supports from MINECO and FEDER (MAT2012-34498, MAT2012-36205 and CTQ2013-40855-R), Generalitat de Catalunya (XRQTC) and CESCA and Gobierno de Aragón - Fondo Social Europeo (research group E40). Support for the research of C.A. was received through the prize "ICREA Academia" for excellence in research funded by the Generalitat de Catalunya.

References

1. X. Yan, P. Zhu and J. Li, *Chem. Soc. Rev.*, 2010, **39**, 1877.
2. S. Flemming and R. V. Ulijn, *Chem. Soc. Rev.*, 2014, **43**, 8150.
3. S. Bai, C. Pappas, S. Debnath, P. W. J. M. Frederix, J. Leckie, S. Fleming and R. V. Ulijn, *ACS Nano*, 2014, **8**, 7005.
4. J. Shi, Y. Gao, Z. Yang and B. Xu, *Beilstein J. Org. Chem.*, 2011, **7**, 167.

5. R. J. Williams, A. M. Smith, R. Collins, N. Hodson, A. K. Das and R. V. Ulijn, *Nat. Nanotechnol.*, 2009, **4**, 19.

6. A. M. Smith, R. J. Williams, C. Tang, P. Coppo, R. F. Collins, M. L. Turner, A. Saiani and R. V. Ulijn, *Adv. Mater.*, 2008, **20**, 37.

7. V. Castelletto, C. M. Moulton, G. Cheng, I. W. Hamley, M. R. Hicks, A. Rodger, D. E. López-Pérez, G. Revilla-López and C. Alemán, *Soft Matter*, 2011, **7**, 11405.

8. A. K. Das, R. Collins and R. V. Ulijn, *Small*, 2008, **4**, 279.

9. V. Jayawarna, M. Ali, T. A. Jowitt, A. F. Miller, A. Saiani, J. E. Gough and R. V. Ulijn, *Adv. Mater.*, 2006, **18**, 611.

10. D. E. López-Pérez, G. Revilla-López, I. W. Hamley and C. Alemán, *Soft Matter*, 2013, **9**, 11021.

11. Z. Yang, H. Gu, D. Fu, P. Gao, J. K. Lam and B. Xu, *Adv. Mater.*, 2004, **16**, 1440.

12. M. Reches and E. Gazit, *Science*, 2003, **300**, 625.

13. M. Reches, Y. Porat and E. Gazit, *J. Biol. Chem.*, 2002, **277**, 35475.

14. M. Reches and E. Gazit, *Nano Lett.*, 2004, **4**, 581.

15. N. Amdursky, E. Gazit and G. Rosenman, *Adv. Mater.*, 2010, **22**, 2311.

16. A. Mahler, M. Reches, M. Rechter, S. Cohen and E. Gazit, *Adv. Mater.*, 2006, **18**, 1365.

17. J. Raeburn, C. Mendoza-Cuenca, B. N. Cattoz, M. A. Little, A. E. Terry, A. Z. Cardoso, P. C. Griffiths and D. J. Adams, *Soft Matter*, 2015, **11**, 927.

18. S. Debnath, A. Shome, D. Das and P. K. Das, *J. Phys. Chem. B*, 2010, **114**, 4407.

19. T. H. Han, T. Ok, J. Kim, D. O. Shin, H. Ihee, H.-S. Lee and S. O. Kim, *Small*, 2010, **6**, 945.

20. L. Chronopoulou, S. Lorenzoni, G. Masci, M. Dentini, A. R. Togna, G. Togna, F. Bordi and C. Palocci, *Soft Matter*, 2010, **6**, 2525.

21. E. Mayans, G. Ballano, J. Casanovas, A. Díaz, A. Pérez-Madrigal, F. Estrany, J. Puiggalí, C. Cativiela and C. Alemán, *Chem. Eur. J.*, 2015, **21**, 16895.

22. P. P. Sharma, B. Rathi, J. Rodrigues and N. Y. Gorobets, *Curr. Topics Med. Chem.*, 2015, **15**, 1268.

23. V. E. Santo, M. E. Gomes, J. F. Mano and R, L. Reis, *Nanomedicine*, 2012, **7**, 1045.

24. A. Amdursky, P. Beker, J. Schklovsky, E. Gazit and G. Rosenman, *Ferroelectrics*, 2010, **399**, 107.

25. M. Reches and E. Gazit, *Phys. Biol.*, 2006, **3**, S10.

26. C. Tang, A. M. Smith, R. F. Collins, R. V. Ulijn and A. Saiani, *Langmuir*, 2009, **25**, 9447.

27. S. M. M. Reddy, G. Shanmugam, N. Duraipandy, M. S. Kiran and A. B. Mandal, *Soft Matter*, 2015, **11**, 8126.

28. H. Takayasu, *Fractals in the Physical Sciences*, Manchester University Press, Manchester and New York, 1990, pp 11–17.

29. W. Rasband, NIH, Fractal box counting method using ImageJ, http://www.nist.gov/lispix/doc/fractal/image-java--box-count.htm, accessed: December, 2015.

30. M. J. Frisch, G. W. Trucks, H. B. Schlegel, G. E. Scuseria, M. A. Robb, J. R. Cheeseman, G. Scalmani, V. Barone, B. Mennucci, G. A. Petersson, H. Nakatsuji, M. Caricato, X. Li, H. P. Hratchian, A. F. Izmaylov, J. Bloino, G.

Zheng, J. L. Sonnenberg, M. Hada, M. Ehara, K. Toyota, R. Fukuda, J. Hasegawa, M. Ishida, T. Nakajima, Y. Honda, O. Kitao, H. Nakai, T. Vreven, J. A. Montgomery Jr., J. E. Peralta, F. Ogliaro, M. Bearpark, J. J. Heyd, E. Brothers, K. N. Kudin, V. N. Staroverov, R. Kobayashi, J. Normand, K. Raghavachari, A. Rendell, J. C. Burant, S. S. Iyengar, J. Tomasi, M. Cossi, N. Rega, J. M. Millam, M. Klene, J. E. Knox, J. B. Cross, V. Bakken, C. Adamo, J. Jaramillo, R. Gomperts, R. E. Stratmann, O. Yazyev, A. J. Austin, R. Cammi, C. Pomelli, J. W. Ochterski, R. L. Martin, K. Morokuma, V. G. Zakrzewski, G. A. Voth, P. Salvador, J. J. Dannenberg, S. Dapprich, A. D. Daniels, O. Farkas, J. B. Foresman, J. V. Ortiz, J. Cioslowski, D. J. Fox, Gaussian 09, Revision A.02. *Gaussian Inc.* 2009.

31. Y. Zhao and D. G. Truhlar, *Theor. Chem. Acc.*, 2008, **120**, 215.
32. Y. Zhao and D. G. Truhlar, *J. Chem. Phys.*, 2006, **125**, 194101.
33. B. Teixeira-Dias, C. Alemán, F. Estrany, D. S. Azambuja and E. Armelin, *Electrochim. Acta*, 2011, **56**, 5836.
34. M. Du, P. Zhu, X. Ya, Y. Su, W. Song and J. Li, *Chem. Eur. J.*, 2011, **17**, 4238.
35. M. Hughes, H. Xu, P. W. J. M. Frederix, A. M. Smith, N. T. Hunt, T. Tuttle, I. A. Kinloch and R. V. Ulijn, *Soft Matter*, 2011, **7**, 10032.
36. C. H. Görbitz, *Chem. Commun.*, 2006, 2332.
37. X. Yan, J. Li and H. Möhwald, *Adv. Mater.*, 2011, **23**, 2796.
38. H. Cölfen and S. Mann, *Angew. Chem. Int. Ed.*, 2003, **42**, 2350.
39. X. H. Yan, Y. Cui, Q. He, K. W. Wang, J. B. Li, W. H. Mu, B. L. Wang and Z. C. Ou-yang, *Chem. Eur. J.*, 2008, **14**, 5974.
40. V. V. Korolkov, S. Allen, C. J. Roberts and S. J. B. Tendler, *Faraday Discuss.*, 2013, **166**, 257.

41. T. H. Han, J. K. Oh, G.-J. Lee, S. II Pyun and S. O. Kim, *Colloids Surf. B*, 2010, **79**, 440.

42.

43. P. Zhu, X. Yan, Y. Su, Y. Yang and J. Li, *Chem. Eur. J.*, 2010, **16**, 3176.

44. W. Wang and Y. Chau, *Soft Matter*, 2009, **5**, 4893.

45. L. Gránásy, T. Pusztai, T. Börzsönyi, J. A. Warren and J. F. Douglas, *Nat. Mater.*, 2004, **3**, 645.

46. L. Gránásy, T. Pusztai, T. Börzsönyi, G. Tóth, G. Tegze, J. A. Warren and J. F. Douglas, *J. Mater. Res.*, 2006, **21**, 309.

47. V. Ferreiro, J. F. Douglas, J. A. Warren and A. Karim, *Phys. Rev. E*, 2002, **65**, 051606.

48. J. Peng, Y. Xuan, H. Wang, B. Li and Y. Han, *Polymer*, 2005, **46**, 5767.

49. B. B. Mandelbrot, *The Fractal Geometry of Nature*, Freeman, San Francisco, CA, USA, 1982.

50. T. A. Witten and L. M. Sander, *Phys. Rev. Lett.*, 1981, **47**, 1400.

51. P. Meakin, *Phys. Rev. A*, 1983, **27**, 604.

52. D. Zanuy, I. W. Hamley and C. Alemán, *J. Phys. Chem. B*, 2011, **115**, 8937.

53. A. Barth and C. Q. Zscherp, *Rev. Biophys.*, 2002, **35**, 369.

54. H. Rapaport, H. Grisaru and T. Silberstein, *Adv. Funct.Mater.*, 2008, **18**, 2889.

55. T. Steckmann, Z. Awan, B. S. Gerstman, P. P. Chapagain, *J. Theor. Biol.*, 2012, **301**, 95.

56. C. H. Görbitz, *Chem. Eur. J.*, 2001, **7**, 5153–5159.

57. P. Kumaraswamy, R. Lakshmanan, S. Sethuraman and U. Maheswari, *Soft Matter*, 2011, **7**, 2744.

58. P. Tamamis, E. Gazit, G. Archontis, U. H. E. Hansmann, J. H. Meinke, S. Mohanty and W. Nadler, in *From Computational Biophysics to Systems Biology 2008 (CBSB08)* (Eds: P. Tamamis and L. Adler-abramovich), pp 393-396

59. C. Guo, Y. Luo, R. Zhou and G. Wei, *Nanoscale*, 2014, **6**, 2800.

60. C.-A. Palma, M. Cecchini and P. Samori, *Chem. Soc. Rev.*, 2012, **41**, 3713.

61. U. K. Weber, V. M. Burlakov, L. M. A. Perdigao, R. H. J. Fawcett, P. H. Beton, N. R. Champness, J. H. Jefferson, G. A. D. Briggs and D. G. Pettifor, *Phys. Rev. Lett.*, 2008, **100**, 156101.

CAPTIONS TO FIGURES

Figure 1. Scheme of the coupling reactions used to obtain FFFF-OFm. *i)* Boc-L-Phe-OH, Fmoc chloride, *N*-ethyldiisopropylamine (DIPEA), 4-dimethylaminopyridine (DMAP), CH_2Cl_2. *ii)* CF_3COOH (TFA)/CH_2Cl_2 1/1. *iii) N*-[3-(dimethylamino)-propyl]-*N*'-ethylcarbodiimide hydrochloride (EDC·HCl)/1-hydroxy-7-azabenzotriazole (HOBt), *N*-methylmorpholine (NMM; to keep pH 8), CH_2Cl_2.

Figure 2. For Fmoc-FF-OFm assemblies, SEM micrographs and/or AFM images of: (a) stacked braids obtained in 2:3 HFIP:water at 4ºC using a peptide concentration of 2 mg/mL without and with application of a sonication bath treatment to the peptide solution; (b) stacked braids obtained in 1:9 HFIP:water at 4ºC using a peptide concentration of 0.5 mg/mL. The window size for the 3D topographic and 2D amplitude AFM images is 20×20 μm^2; (c) doughnut-like microstructures obtained in 4:1 HFIP:water at 4ºC using a peptide concentration of 4 mg/mL . The 3D topographic AFM image corresponds to a window of 25×15 μm^2.

Figure 3. For Fmoc-FF-OFm assemblies, SEM micrographs and/or AFM images of microtubes obtained in: (a) 4:1 HFIP:^{i}PrOH at room temperature using a peptide concentration of 4 mg/mL (windows of 2D and 3D AFM images are 15×15 μm^2 and 5×5 μm^2, respectively); (b) 4:1 HFIP:acetone at 4 ºC using a peptide concentration of 3.44 mg/mL. SEM micrographs of bundled nanotubes arrays are also displayed in (b).

Figure 4. For Fmoc-FFF-OFm assemblies, SEM micrographs and/or AFM images of: (a) stacked braids obtained in 1:4 HFIP:water at 4 ºC using a peptide concentration of 1 and 0.05 mg/mL (left and right, respectively); (b) Corkscrew-like morphology obtained in 2:3 HFIP:EtOH at 4 ºC using a peptide concentration of 2 mg/mL; (c) Corkscrew-like morphology attached to a micro-conical hollow structure obtained in 1:4 HFIP:EtOH at 4 ºC using a peptide concentration of 1 mg/mL. The magnified SEM

micrograph and the 3D AFM images evidence that this structure is made of stacked platelets; (d) Submicrometric tubes obtained in 1:99 HFIP:water at 4ºC using a peptide concentration of 0.05 mg/mL (low and high magnification micrographs at left and right, respectively).

Figure 5. For Fmoc-FFF-OFm assemblies, SEM micrographs and/or AFM images of: (a) spherulitic craters obtained in 4:1 HFIP:water at 4 ºC using a peptide concentration of 4 mg/mL (windows of 3D topographic and phase AFM images are 32×32 μm^2); (b) Micrometric spherulites obtained in HFIP at 4 ºC using a peptide concentration of 5 mg/mL (low and high magnification micrographs at left and center, respectively, while birefringence with positive and negative staining is displayed in the optical micrograph at right).

Figure 6. For Fmoc-FFFF-OFm assemblies: (a) optical micrographs and AFM phase images (60×60 and 75×75 μm^2 windows for regions marked with red and light blue squares, respectively) of ultra-thin dentridic structures obtained in 1:49HFIP:water at 4 ºC using a peptide concentration of 0.1 mg/mL and after 20 min sonication. The drop was covered with a coverslip and sprinkled over the glass slide; (b) SEM micrograph of stacked braids obtained in 1:99 HFIP:EtOH at 4ºC using a peptide concentration of 0.05 mg/mL. The length and surface topography of individual stacked elements is displayed in SEM micrographs and the 3D AFM image (10×5 μm^2 window), respectively.

Figure 7. Typical dendritic microstructures obtained for Fmoc-FFFF-OFm HFIP:EtOH solutions at room temperature. Optical micrographs (left column) and both 2D and 3D AFM images (center and right columns, respectively) correspond to peptide concentrations and HFIP:EtOH mixtures of: 0.5 mg/mL and 1:9 (first row); 1 mg/mL and 1:4 (second row); and 2 mg/mL and 2:3 (third row). Samples were prepared by sonicating the initial stock solution during 50 min. Branching angle for the growth

primary framework and dendritic branches are displayed in the 2D AFM image of the microstructure formed using a 1 mg/mL peptide solution.

Figure 8. Analysis of the fractal dimension using the box-counting method for the Fmoc-FFFF-OFm dendritic microstructures displayed in Figures 7. The binary images used for such analysis are displayed in Figure S8. The fractal dimension is related to the slope of adjusted equations (see text).

Figure 9. Lowest energy (a) antiparallel and (b) parallel assemblies predicted for three Fmoc-FF-OFm strands using M06L/6-31G(d) calculations. Both lateral (left) and top (right) views are provided. Aliphatic and aromatic hydrogen atoms have been omitted for clarity while intermolecular hydrogen bonds in the β-sheet are represented by dashed lines. Relevant energetic information for these two assemblies is displayed in Table 2.

Table 1. Description of the conditions required by Fmoc-FF-OFm, Fmoc-FFF-OFm and Fmoc-FFFF-OFm to form different morphologies.

Peptide	Solvent	Concentration (mg/mL)	Temperature (º C)	Morphology
Fmoc-FF-OFm	4:1 HFIP : Water	4	4	Doughnut
	2:3 and 1:9 HFIP:Water	0.5-2.0	4	Stacked-braids
	2:3 HFIP:water	2	4	Dendritic
	1:49 and 1:99 HFIP:MeOH	0.04-0.1	4	Stacked-braids
	1:4 HFIP:EtOH	0.087	4	Dendritic
	4:1 HFIP:^{i}PrOH	3-4	25	Microtubes
	4:1 HFIP:Acetone	3-4	4	Microtubes
Fmoc-FFF-OFm	4:1 HFIP:Water	4	4	Spherulitic craters
	1:4 HFIP:Water	≤ 1	4	Stacked-braids
	1:99 HFIP:Water	0.05	4	Submicrometric tubes
	2:3 and 1:4 HFIP:EtOH	1-2	4	Corkscrew
	1:19 HFIP:EtOH	≤ 0.25	4	Stacked-braids
	1:9 HFIP:^{i}PrOH	≤ 0.5	4	Stacked-braids
	38:11 DMF:MeOH	6.1	25	Submicrometric tubes
	HFIP	3-5	4	Micrometric spherulites
Fmoc-FFFF-OFm	1:24 and 1:49 HFIP:Water	0.1-0.2	4	Ultra-thin dendrimers
	1:4 HFIP:EtOH	0.5-2	25	Dendrimers
	1:9 to 1:99 HFIP:EtOH	0.05-0.5	4	Stacked braids

Table 2. Summary of the results derived from M06L/6-31G(d) calculations on antiparallel and parallel β-sheets of Fmoc-FF-OFm, Fmoc-FFF-OFm and Fmoc-FFFF-OFm: relative energy (ΔE), number of hydrogen bonds in the model with three strands ($\#N_{hbonds}$), hydrogen bonding distance ($d_{H\cdots O}$) and angle (∠N–H···O), interaction energy (ΔE_{int}), and cooperative energy associated with three-body non-additive effects (ΔE_{coop}). Although the number of starting geometries for each peptide was around 20-30, only results for the most stable antiparallel and parallel arrangements are displayed (Figures 9, S9 and S10).

	ΔE (kcal/mol)	**# N_{hbonds}**	**$d_{H\cdots O}$ (Å), ∠N–H···O (º)**	**ΔE_{int} (kcal/mol)**	**ΔE_{coop} (kcal/mol)**
			Fmoc-FF-OFm		
Antiparallel	0.0	4	1.988 Å, 156.2º	-52.8	1.5
Parallel	1.8	4	2.097 Å, 153.7º	-51.0	-7.5
			Fmoc-FFF-OFm		
Antiparallel	0.0	6	1.964 Å, 156.8º	-70.5	-2.9
Parallel	3.3	6	2.028 Å, 154.7º	-67.2	-7.5
			Fmoc-FFFF-OFm		
Antiparallel	0.0	8	1.976 Å, 155.2º	-88.6	-4.9
Parallel	9.8	8	2.016 Å, 153.9º	-78.7	-8.3

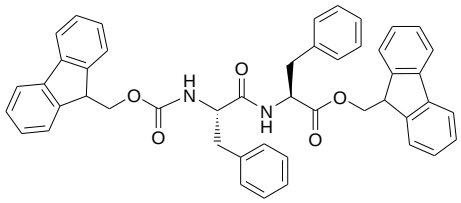

Fmoc-FF-OFm

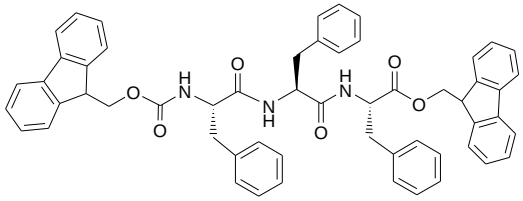

Fmoc-FFF-OFm

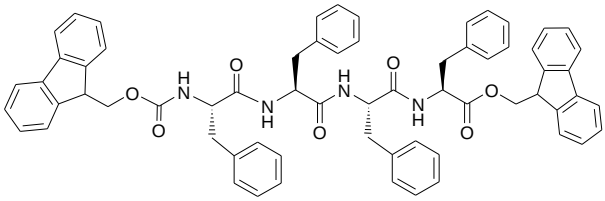

Fmoc-FFFF-OFm

Scheme 1

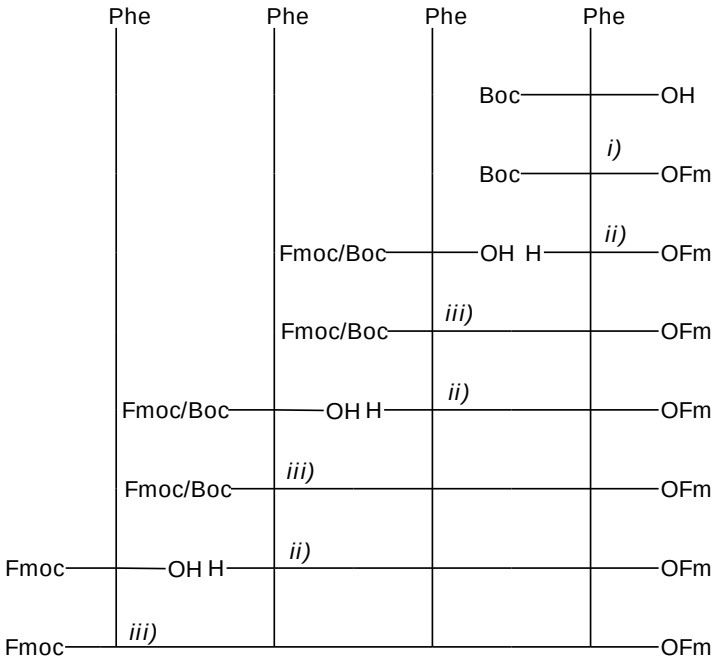
Phe
Phe
Phe
Phe
Boc
OH
i)
Boc
OFm
ii)
Fmoc/Boc
OH H
OFm
iii)
Fmoc/Boc
OFm
ii)
Fmoc/Boc
OH H
OFm
iii)
Fmoc/Boc
OFm
ii)
Fmoc
OH H
OFm
iii)
Fmoc
OFm

Figure 1

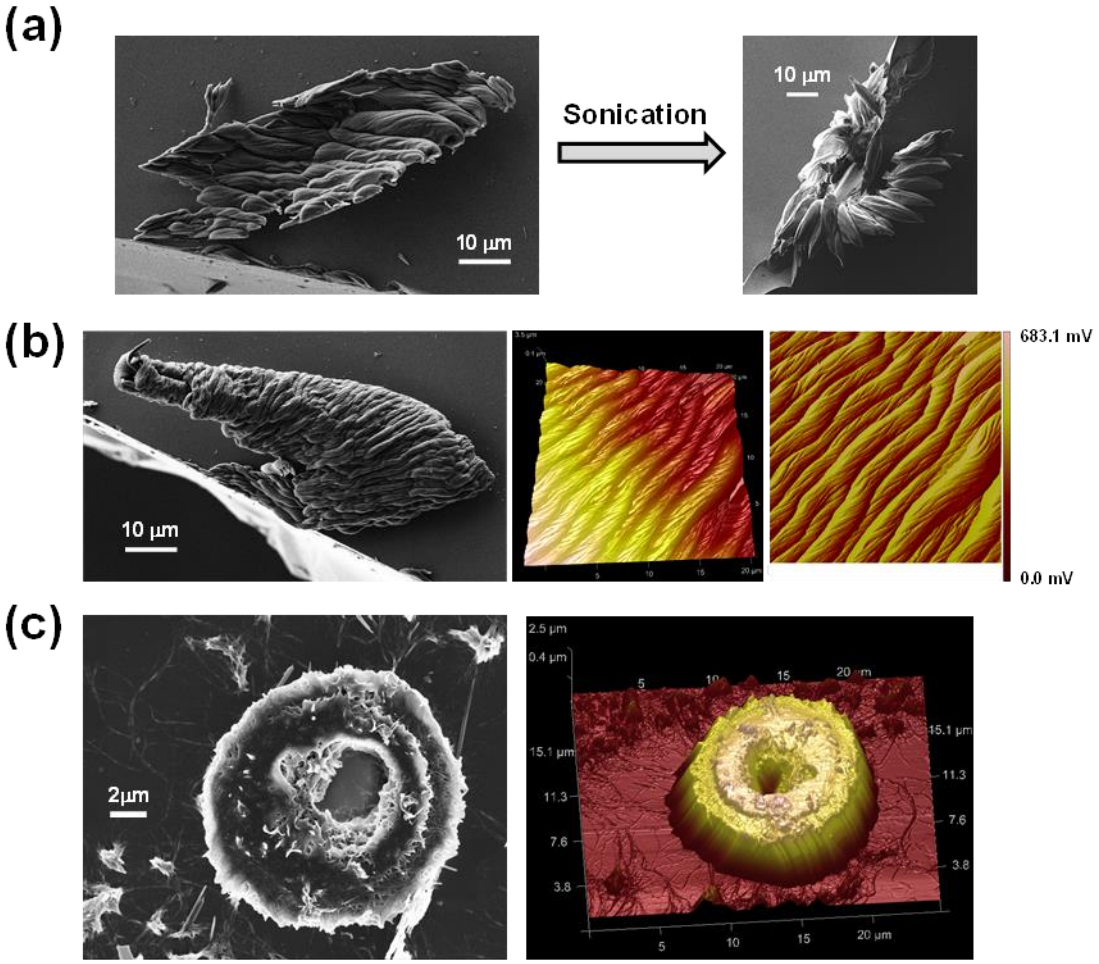
(a)
10 μm
Sonication
10 μm
(b)
10 μm
683.1 mV
0.0 mV
(c)
2μm
2.5 μm
0.4 μm
15.1 μm
11.3
7.6
3.8
5
10
15
20 μm

Figure 2

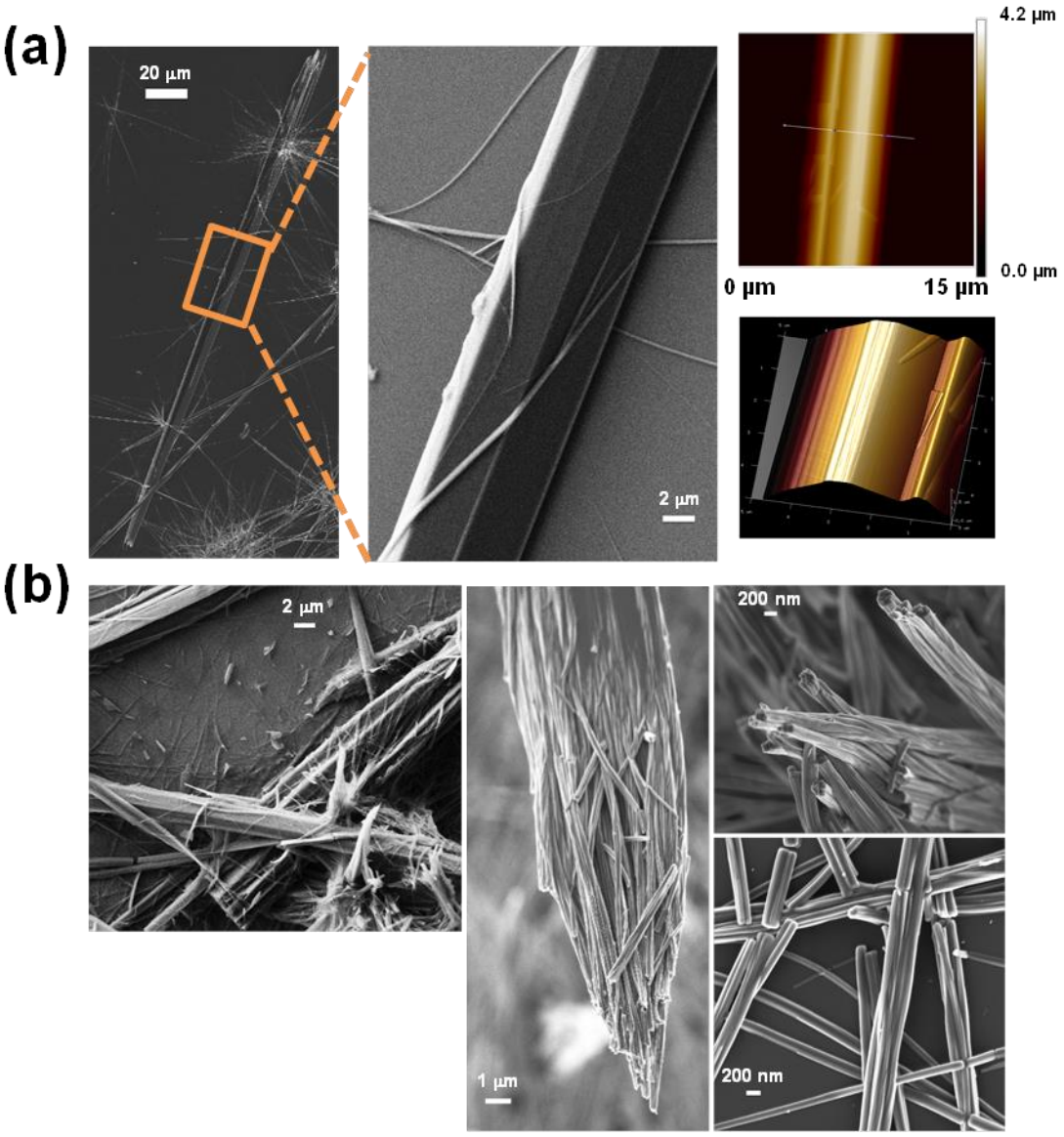

Figure 3

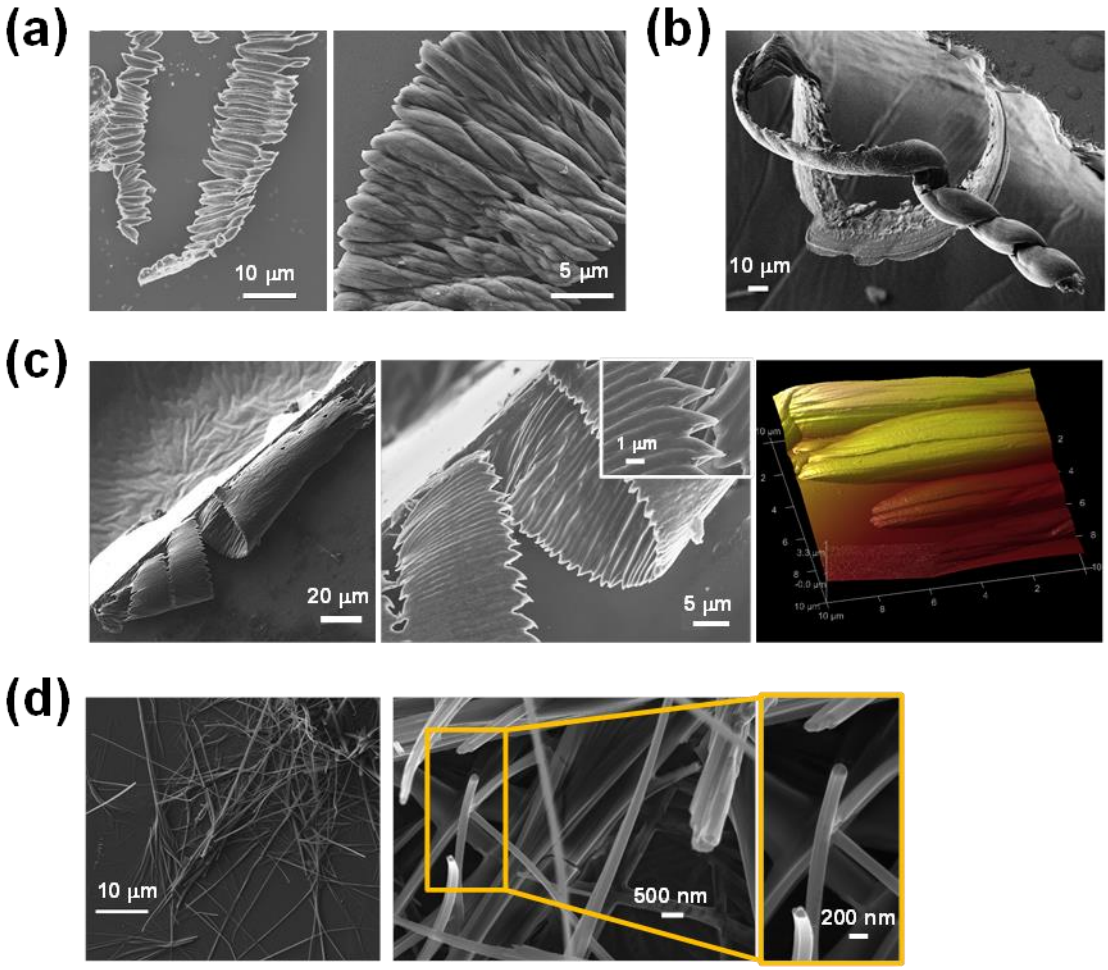

Figure 4

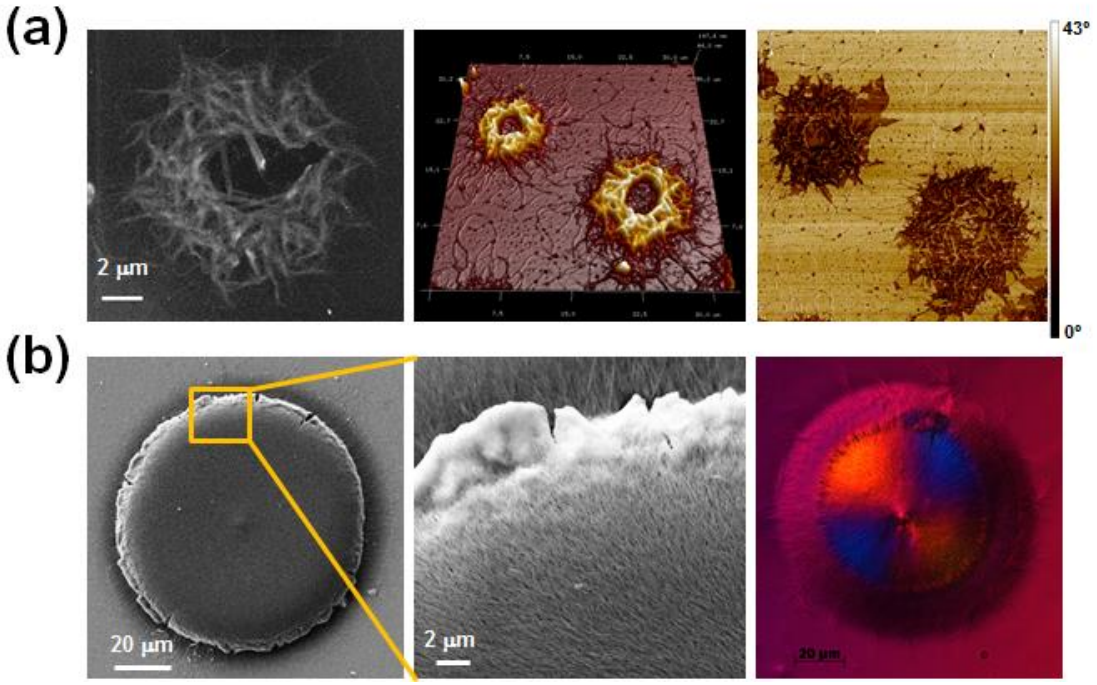

Figure 5

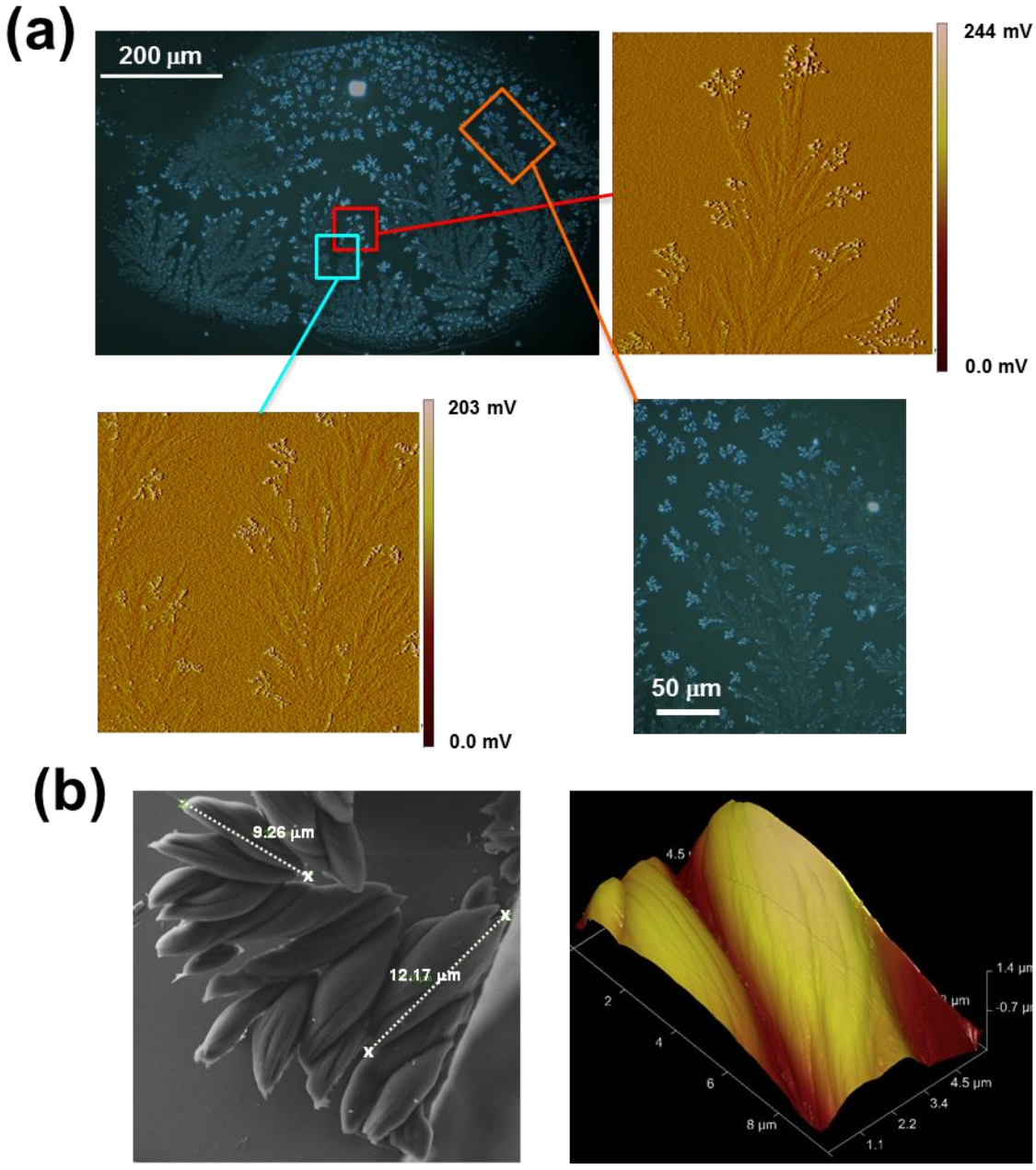
(a)
200 µm
244 mV
0.0 mV
203 mV
0.0 mV
50 µm
(b)
9.26 µm
12.17 µm
4.5
2
4
6
8 µm
4.5 µm
3.4
2.2
1.1
1.4 µm
-0.7 µm

Figure 6

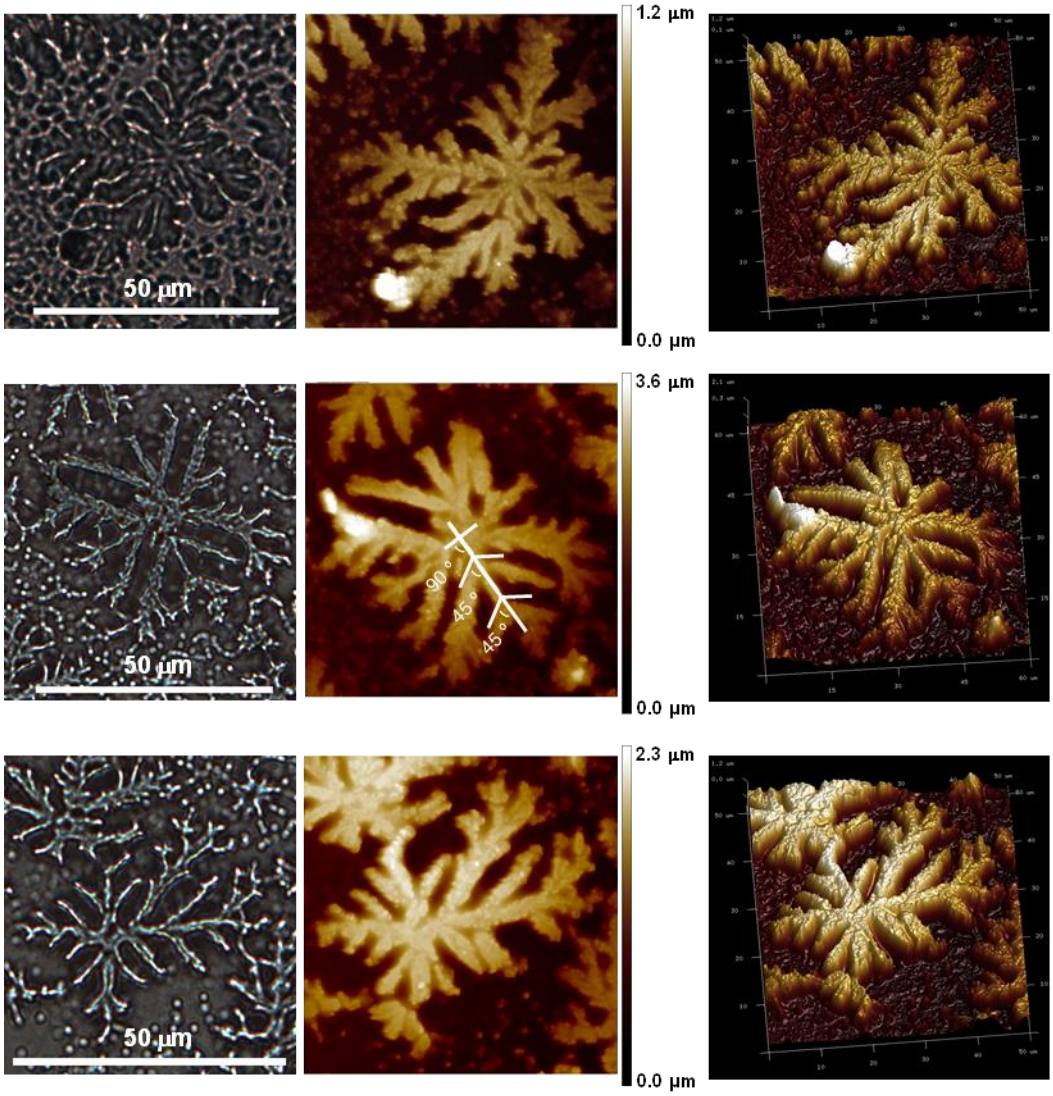

Figure 7

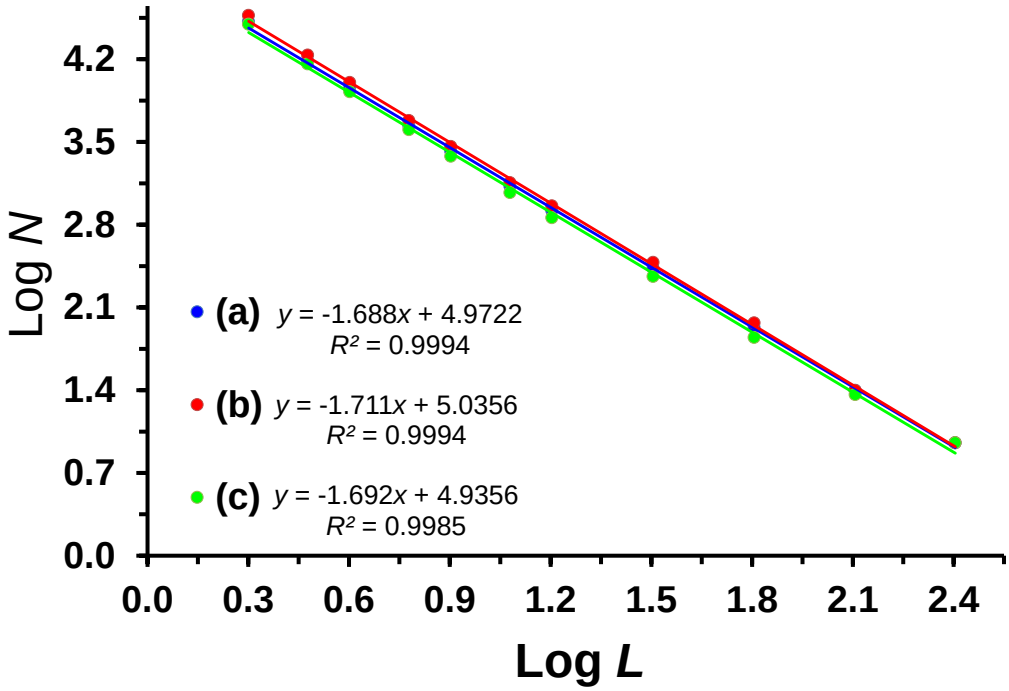
Log N
4.2
3.5
2.8
2.1
1.4
0.7
0.0
0.0
0.3
0.6
0.9
1.2
1.5
1.8
2.1
2.4
Log L
(a) y = -1.688x + 4.9722
R² = 0.9994
(b) y = -1.711x + 5.0356
R² = 0.9994
(c) y = -1.692x + 4.9356
R² = 0.9985

Figure 8

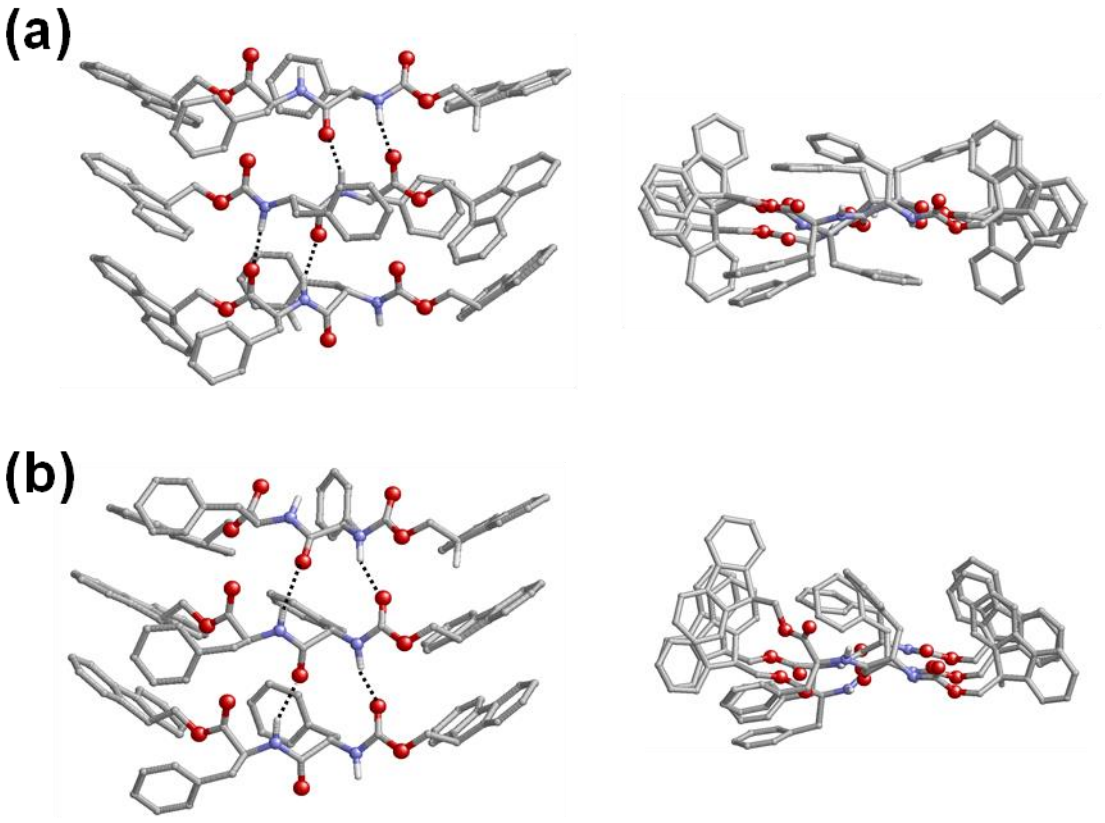

Figure 9

Graphical Abstract